

# InAs-based quantum cascade lasers

J. Devenson, R. Teissier, O. Cathabard, and A. N. Baranov  
 Institut d'Électronique du Sud, UMR5214 CNRS / Université Montpellier 2  
 34095 Montpellier, France

## ABSTRACT

Different issues of the development of short wavelength quantum cascade lasers (QCLs) in the InAs/AlSb system, concerning both optical and electronic design, are considered. A plasmon enhanced waveguide is shown to be suitable for use in InAs-based QCLs operating at wavelengths near 3  $\mu\text{m}$ . High performance lasers emitting near 3.3  $\mu\text{m}$  are demonstrated, as well as short wavelength QCLs emitting down to 2.75  $\mu\text{m}$ . It is shown that their performances are not limited neither by interband absorption across the small band gap of InAs, nor by the electron scattering into the L-minimum of the well material.

**Keywords:** Quantum cascade lasers, infrared lasers

## 1. INTRODUCTION

Quantum cascade lasers (QCLs) are considered now as standard light sources for many chemical sensing applications in the midinfrared above 4  $\mu\text{m}$ . Some spectroscopic applications require injection semiconductor lasers emitting at shorter wavelengths in the vicinity of 3  $\mu\text{m}$ . This spectral region is in principle accessible both for interband diode lasers and quantum cascade lasers (QCLs) operating at room temperature (RT). Performances of diode lasers rapidly degrade above 3  $\mu\text{m}$  due to fundamental limitations such as increasing influence of nonradiative Auger recombination. High quality QCLs based on the InP technology have been demonstrated for  $\lambda > 3.8 \mu\text{m}^{1,2}$  but widening their operation range towards shorter wavelengths is still a challenge due mainly to material limitations. Using adequate materials high performance QCLs operating at wavelengths as short as 3  $\mu\text{m}$  or even below can be developed.

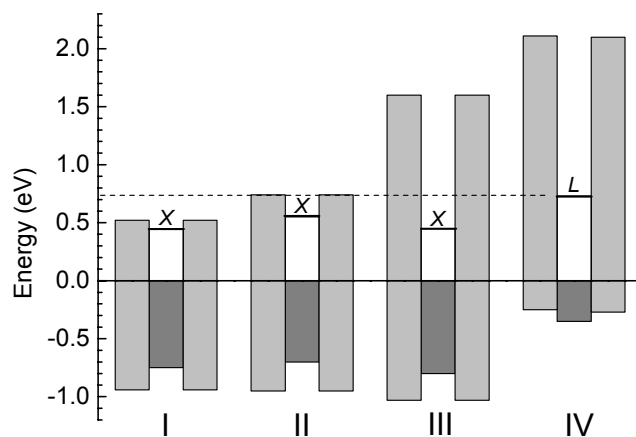


Fig. 1. Band offsets in material systems suitable to fabricate quantum cascade lasers emitting at  $\lambda < 5 \mu\text{m}$ . Energy position of lateral minima, X or L, in the conduction band of the well material is shown.  
 I –  $\text{In}_{0.53}\text{Ga}_{0.47}\text{As}/\text{In}_{0.52}\text{Al}_{0.48}\text{As}/\text{InP}$ ; II -  $\text{In}_{0.7}\text{Ga}_{0.3}\text{As}/\text{In}_{0.4}\text{Al}_{0.6}\text{As}/\text{InP}$ ;  
 III -  $\text{In}_{0.53}\text{Ga}_{0.47}\text{As}/\text{AlSb}_{0.44}\text{As}_{0.56}\text{As}/\text{InP}$ ; IV –  $\text{InAs}/\text{AlSb}/\text{InAs}$

The maximum transition energy of QCLs is limited primarily by the conduction band offset between the well and barrier materials. Band offsets in some material systems suitable to fabricate QCLs emitting at  $\lambda < 5 \mu\text{m}$  are shown in Fig.1. The

invention of QCLs<sup>3</sup> and the most important milestones in their progress are associated with the lattice matched InP-based material system (I in Fig.1). Because of the relatively small conduction band discontinuity of 0.52 eV the wavelength range covered by such QCLs begins at about 4.5  $\mu\text{m}$ .

Another parameter important for realization of short wavelength QCLs is the energy position of lateral minima, X or L, in the conduction band of the well material (Fig.1). If the states related to the lateral bands are close to  $\Gamma$ -states of a QCL they can trap electrons and thus disrupt operation of the device. On the other hand, there are still no clear experimental data on the importance of this effect. An enormous progress in QCL performances and short wavelength operation has been achieved with strain compensated InP based materials. With increasing In content in the wells and Al concentration in the barriers in such structures it is possible to improve both the conduction band offset and  $\Gamma$ -X separation (II in Fig.1). QCL emission near 3.5  $\mu\text{m}$  obtained in this system was for a long time the short wavelength limit of QCL operation<sup>4</sup>. Suitability of this system for short wavelength operation can be improved by employing composite barriers made of InAlAs and AlAs. Low temperature QCL emission down to 3.05  $\mu\text{m}$  has been obtained in such devices<sup>5</sup>. Another solution to obtain short wavelength QCL emission consists in use of AlSbAs barriers lattice matched with InP substrates (III in Fig.1). In this case the conduction band discontinuity is quite large but, as the well material is the same as in the classical InP-based system, the  $\Gamma$ -X separation is small. Nevertheless, QCLs emitting at wavelengths as short as 3.05  $\mu\text{m}$  have been demonstrated in this material system<sup>6</sup> at cryogenic temperatures. The InAs/AlSb material system (IV in Fig.1) seems to be at present the most promising for the development of short wavelength QCLs thanks to the high conduction band offset of 2.1 eV and the large  $\Gamma$ -L distance of 0.73 eV in InAs. Another advantage of this system is the small electron mass in InAs, which is favorable to obtain QCLs with high gain and low threshold. InAs-based QCLs emitting at 2.95  $\mu\text{m}$  at 80 K and operating close to RT have been demonstrated<sup>8</sup>. However, near room temperature operation was barely possible for these devices with very high current densities exceeding 10  $\text{kA}/\text{cm}^2$ . In this paper we consider different issues of the development of short wavelength InAs-based QCLs and present some last achievements in this field.

## 2. WAVEGUIDE

Existing InAs-based QCLs are associated with a plasmon enhanced waveguide<sup>7,8</sup> consisting of n+- InAs cladding layers and low doped InAs spacers around the active zone. Heavy doping provides sufficiently low refractive index of the cladding layers while strong free carrier absorption in this material is compensated by separation of the active zone from these regions using the spacers. This approach becomes not evident at wavelengths shorter than 4  $\mu\text{m}$  because of the small band gap of InAs (0.356 eV at RT).

A dielectric waveguide based on wide gap AlGaSbAs alloys is commonly used in interband diode lasers grown on GaSb emitting up to 3.26  $\mu\text{m}$ <sup>9</sup>. This waveguide, which can potentially provide low loss and high optical confinement, seems to be suitable also for InAs/AlSb QCLs grown on InAs or GaSb. On the other hand, existence of deep levels in AlSb rich alloys results in poor electrical conductivity at low temperatures. Another possible source of instability of the devices is a very high conduction band offset at interfaces between AlGaSbAs and the InAs-based active zone, which requires careful band grading in these regions to reduce the voltage drop and to avoid electrical breakdown of the lasers. Our first InAs/AlSb QCLs with the dielectric waveguide grown on GaSb, which emitted near 3.8  $\mu\text{m}$  at low temperatures, were extremely unstable. Only a few devices had a life time long enough to record an emission spectrum<sup>10</sup>.

We have found the plasmon enhanced waveguide can be successfully employed in InAs-based QCLs operating at wavelengths shorter than 4  $\mu\text{m}$ . The optical bandgap of n-InAs increases quickly with doping due the Moss-Burstein effect. Our photoluminescence measurements show that at doping levels higher than  $8 \cdot 10^{18} \text{cm}^{-3}$  the interband absorption edge of InAs is shifted below 3  $\mu\text{m}$  at RT, which makes possible to use such material in cladding layers of the lasers provided its refractive index is sufficiently low and free carrier absorption is acceptable.

To calculate the refractive index and absorption of doped InAs we used the Drude model taking into account two main contributions to the dielectric function: lattice absorption (optical phonon effect) and free carrier absorption (plasma effect).

The dielectric function can be written<sup>11</sup>:

$$(n + ik)^2 = \varepsilon(\omega) = \varepsilon_\infty \left[ 1 - \frac{\omega_p^2}{\omega(\omega + i\gamma)} + \frac{\omega_L^2 - \omega_T^2}{\omega_T^2 - \omega^2} \right] \quad (1)$$

where  $\omega_p$  is the plasma frequency, given by :

$$\omega_p = \frac{Ne^2}{m^* m_0 \varepsilon_\infty} \quad (2)$$

$N$  is electron concentration,  $\omega_L$  is the longitudinal resonance frequency ( $\omega_L = 243.3\text{cm}^{-1}$ ),  $\omega_T$  is the transverse resonance frequency ( $\omega_T = 218.9\text{cm}^{-1}$ ),  $\varepsilon_\infty = 12.25$  is the high frequency dielectric constant and  $\gamma^{-1}$  is the scattering time of the free carriers by phonons, defined as:

$$\gamma = \frac{e}{m^* m_0 \mu} \quad (3)$$

where  $m^*$  is the effective electron mass and  $\mu$  is the electron mobility in InAs. The values of the refractive index and absorption are then deduced from :

$$\begin{aligned} N(\omega) &= \sqrt{\varepsilon(\omega)} \\ n(\omega) &= \text{Re}[N(\omega)] \\ k(\omega) &= \text{Im}[N(\omega)] \end{aligned} \quad (4)$$

The electron concentration and mobility were measured by the Van der Pauw technique on samples grown on undoped GaAs, the electron effective mass was extracted from the experimentally found plasma frequency.

The calculations show that to provide efficient optical confinement in InAs/AlSb QCLs emitting near  $3 \mu\text{m}$  the doping level of n-InAs cladding layers should be considerably increased compared with reported QCL emitting at  $\lambda > 4.5 \mu\text{m}$ <sup>12</sup> up to more than  $2 \cdot 10^{19} \text{cm}^{-3}$  (Fig.2). On the other hand, the required increase in the doping level results in comparable or even weaker free carrier absorption since it decreases as  $\lambda^{-2}$  at short wavelengths (Fig.2). Nevertheless, in order to obtain low waveguide loss the active zone should be separated from the cladding layers. Low doped InAs can not be used for this purpose below  $4 \mu\text{m}$  because of its small band gap. We proposed to replace it by short period InAs/AlSb superlattices consisting typically of (2.5-2) nm InAs + (1.5-2) nm AlSb with optical band gaps high enough to avoid interband absorption at  $\lambda \sim 3 \mu\text{m}$ . The spacer thickness and the doping level of the cladding layers should be carefully optimized to provide efficient optical confinement and acceptable loss at targeted emission wavelengths.

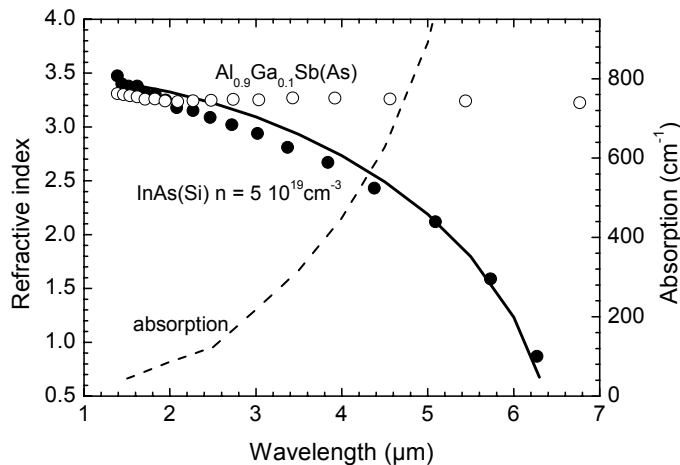


Fig. 2. Refractive index of n+-InAs grown on GaAs (solid circles) and  $\text{Al}_{0.9}\text{Ga}_{0.1}\text{Sb(As)/GaSb}$  (open circles) measured at room temperature as a function of wavelength. Calculated refractive index and free carrier absorption for n+-InAs are represented by solid and dashed curves, respectively.

Refractive index of different materials which can be used in the waveguide of InAs-based QCLs was obtained from reflectivity spectra measured using Nicolet Nexus 860 infrared Fourier transform spectrometer (FTIR). Positions of interference fringes in the spectra were used to extract the refractive index at corresponding wavelengths. This procedure gives quite accurate information on refractive index in a large spectral range, except in the vicinity of critical points of high index dispersion near energy gaps in the studied material or in the substrate. The reflectivity spectra permitted also to find the plasma frequency in heavily doped n-InAs samples which was used in calculations of optical constants of this material.

The  $\text{Al}_{0.9}\text{Ga}_{0.1}\text{Sb}(\text{As})$  alloy lattice matched with GaSb, commonly used to form cladding layers in GaSb-based diode lasers, exhibits nearly constant refractive index close to 3.25 in the whole studied spectral range between 1.5 and 7  $\mu\text{m}$  (Fig.2). Refractive index of n-InAs decreases with doping and with wavelengths when approaching the plasma resonance, in fair agreement with the calculated data (Fig.2). For doping levels above  $2 \cdot 10^{19} \text{ cm}^{-3}$  it is lower than that of the quaternary alloy in the spectral region of our interest near 3  $\mu\text{m}$ .

In order to model the laser waveguide it is necessary also to know optical constants of the active zone and spacers, both regions made, in our case, of short period superlattices. To calculate their properties we have to decide if they should be considered as multicomponent alloys or as a mixture of constituent binary compounds. The first assumption is valid in case of strong diffusion or when the superlattice period is comparable with the lattice parameter of its components, otherwise the latter one is applicable. The refractive index of an (InAs 2 nm + AlSb 2 nm) superlattice which we use as spacers in our short wavelength QCLs was measured by the technique described above (Fig.3). The figure shows also photoluminescence spectra of the sample indicating band gaps of the superlattice and the InAs substrate at 1.7 and 3.6  $\mu\text{m}$ , respectively. In spite of perturbations of the measurements near these points, the data give a good idea about the refractive index of the material in a large spectral range.

The refraction index calculated as average values of InAs and AlSb indices is shown in Fig.3, as well as theoretical data for the  $\text{In}_{0.5}\text{Al}_{0.5}\text{As}_{0.5}\text{Sb}_{0.5}$  alloy. As one can see, the average refractive index agrees well with the measured values between 2.5 and 5  $\mu\text{m}$ , at longer wavelengths the experimental data tend to approach the alloy limit. The average index model is also applicable to the active zone of InAs/AlSb QCLs because its layer thicknesses are comparable or greater than those in the studied superlattice. The refractive index of the active zone is usually higher compared with the superlattice spacers due to smaller fractions of low index AlSb.

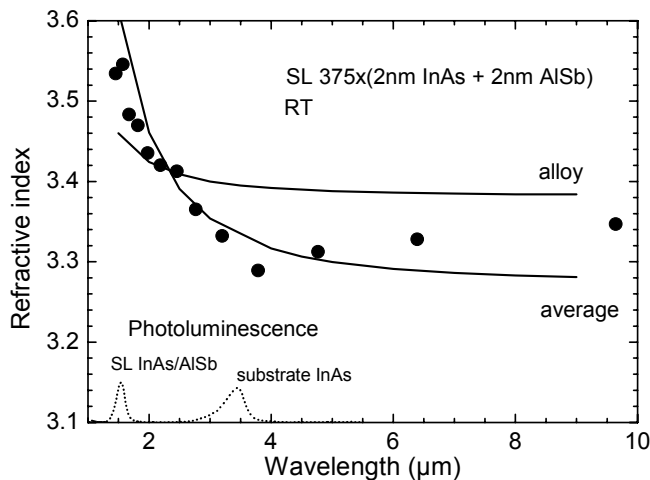


Fig. 3. Refractive index of an undoped InAs/AlSb superlattice grown on InAs measured at room temperature as a function of wavelength (solid circles). Solid lines show data calculated using different assumptions. Photoluminescence spectrum displayed by dotted curves indicates spectral regions where the experimental data are perturbed by the vicinity of energy gaps in the sample.

A typical waveguide which we employed in the InAs/AlSb QCLs emitting near 3  $\mu\text{m}$  consists of 1.8- $\mu\text{m}$ -thick n<sup>+</sup>-InAs cladding layers doped to  $(3-5) \cdot 10^{19} \text{ cm}^{-3}$  and 0.6- $\mu\text{m}$ -thick superlattice spacers around the (1.4-1.6)- $\mu\text{m}$ -thick active zone. The waveguide is characterized by high optical confinement of (50-55) % and low internal loss of  $(4-6) \text{ cm}^{-1}$  calculated considering only free carrier absorption in passive regions.

### 3. MBE GROWTH

Performances of InAs/AlSb QCLs are more growth depended compared with InP-based devices because of absence of common atoms at well/barrier interfaces. Existence of In-Sb or Al-As bonds at interfaces induces high strains and affects crystalline quality of the QCL structure, its average lattice parameter and electronic properties. During MBE growth the quality of InAs/AlSb interfaces can be controlled using special shutter sequences favoring formation of a desired type of the bonds<sup>13</sup>. The use of different growth conditions, including also variation of the V/III flux ratio, results in difference, sometimes significant, in performances of QCLs with nominally the same design. These variations are due to the growth induced deviations in the QCL band profile and to the change in concentration of impurities and deep levels. Deliberate introduction of As into AlSb layers gives an additional possibility to keep lattice mismatch between the structure and the substrate below the relaxation limit.

Short wavelength QCLs containing very thin, (6-20) Å thick, layers are very sensitive to such growth effects as segregation and interdiffusion. High resolution transmission electron microscopy (TEM) studies performed on early InAs/AlSb QC structures revealed very diffused boundaries between InAs and AlSb layers with the length of the transition regions exceeding 10 Å<sup>14</sup>. The resulted smoothed band profile makes difficult to model InAs-based QCLs adequately.

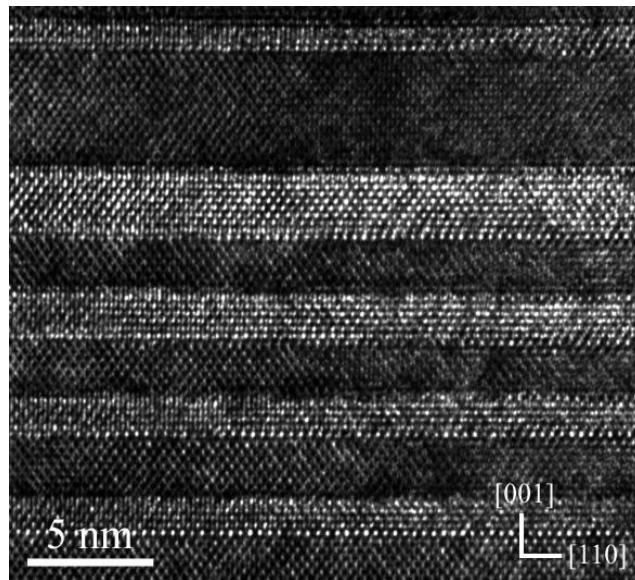


Fig. 4. TEM image of an InAs/AlSb QCL structure. Part of the active zone close to the injection barrier is shown. Dark zones correspond to InAs. (courtesy of Anne Ponchet and Christophe Gatel, CEMES/CNRS, Toulouse, France)

Optimization of MBE growth of such structures permitted to improve considerably their quality. Fig.4 shows a TEM image of one of our recent QCL structures. This picture demonstrates sharp interfaces and absence of significant interdiffusion and segregation in the structure, which allows reliable modeling of the devices.

Our QCL structures were grown on n-InAs (100) substrates in a Riber Compact 21 solid source MBE machine equipped with As and Sb valved cracker cells. InAs cladding layers and InAs layers in the superlattice spacers were doped with silicon while active regions of the lasers were tellurium-doped using an Sb<sub>2</sub>Te<sub>3</sub> effusion cell. The use of tellurium for doping of the active region was found to provide more reproducible results compared with silicon. The InAs and AlSb growth rates of 1 Å/s were used typically in the active region and the spacers, the cladding layers were grown at 1 μm/h. The growth rate of InAs in the active region could be varied in the range 0.9-1.1 Å/s in different structures in order to shift QCL emission from the wavelength corresponding to the nominal design. The real growth rates of both AlSb and InAs could be extracted from X-ray diffraction data comparing superperiods corresponding to the active region and the superlattice spacers. Usually their deviation from the targeted values is less than 2%.

## 4. LASERS

In the first 3  $\mu\text{m}$  QCLs we used a scheme which allowed to achieve RT operation of InAs-based lasers emitting at longer wavelengths<sup>12</sup>. All these devices exhibited quick degradation of performances with temperature. Careful analysis of their characteristics showed that they suffered from backfilling of lower states of the laser transition, which resulted in poor performances at RT. We modified the design of the active zone in order to reduce this effect. This approach was first tried on QCLs emitting above 4  $\mu\text{m}$  and then applied to short wavelength QCLs.

Several QCLs for emission at different wavelengths near 3  $\mu\text{m}$  have been grown. The wavelength of 3.3  $\mu\text{m}$  was chosen as a very important one for molecular spectroscopy of hydrocarbons (wafer D385). The wafers D391 and D392 designed to emit near 2.8 and 2.9  $\mu\text{m}$ , respectively, were grown to explore short wavelength limits of operation of InAs-based QCLs. All the structures had a similar design, the same doping level and the same thickness of the injection barrier.

The active zone of the wafer D391 consists of 25 repeats of the following layer sequence: **27/42/12/38/12/33/12/28/11/25/11/23/11/21/11/21/13/21.5/15/20.5/17/19.5/18/18.5/20/18.8**, (in  $\text{\AA}$  and starting from the injection barrier), where AlSb layers are in bold and Te-doped layers ( $n = 3 \cdot 10^{17} \text{ cm}^{-3}$ ) are underlined. The design of the structure, typical for this series, is depicted in Fig.5. It is based on a vertical transition in three active quantum wells and a funnel injector that aligns at higher electric field as compared to our previous designs.

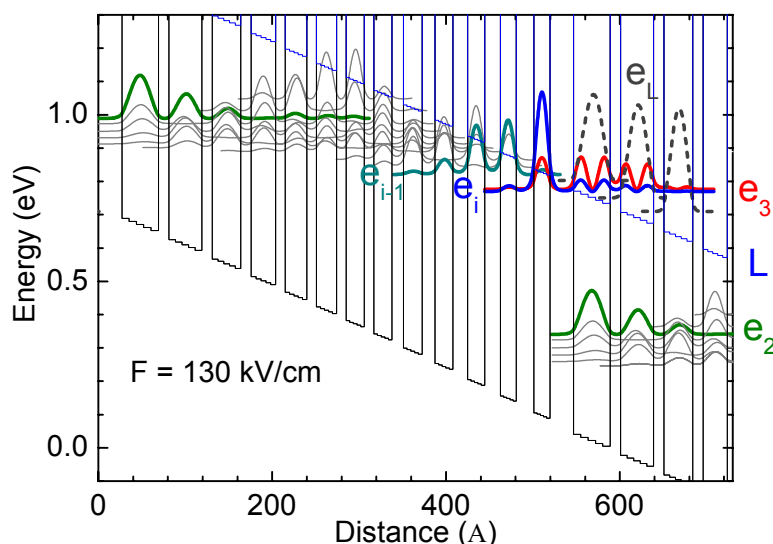


Fig. 5. Conduction band diagram of the active region of the D391 laser at 80 K. Solid curves represent the moduli squared of the relevant electron wave functions. Dotted lines correspond to levels  $e_L$  associated with the L-valley (L) calculated using a  $\Gamma$ -L separation value of 0.73 eV.

The wafers were processed into deep mesa lasers with ridge width of 12 - 20  $\mu\text{m}$  by conventional photolithography and wet chemical etching. Hard baked photoresist was used to protect mesa edges and to planarize the surface. The devices were soldered epi-side down onto copper heat sinks. The back facet of part of the devices was high reflectivity (HR) coated using 500 nm  $\text{SiO}_2$  / 10 nm Cr / 100 nm Au. The lasers were tested in pulsed mode at a repetition rate of 1 kHz and pulse duration of 100 ns. Emission spectra of the lasers were measured using the FTIR with a pyroelectric detector. The spectrometer used in the rapid scan regime was synchronized with the laser driver to obtain clean spectra free of ghosts. In this case the current pulse frequency was 10 kHz, defined by the FTIR scan rate, and the pulse width was 40 ns. Emitted optical power was collected with an  $f/1$  parabolic mirror and measured using a pyroelectric detector calibrated for the used duty cycle.

The QCLs fabricated from the wafer D385 emitted at 3.33  $\mu\text{m}$  at RT. As compared to the previously reported devices emitting at similar wavelength<sup>15</sup>, the temperature behaviour of the present QCLs is significantly improved (Fig.6).

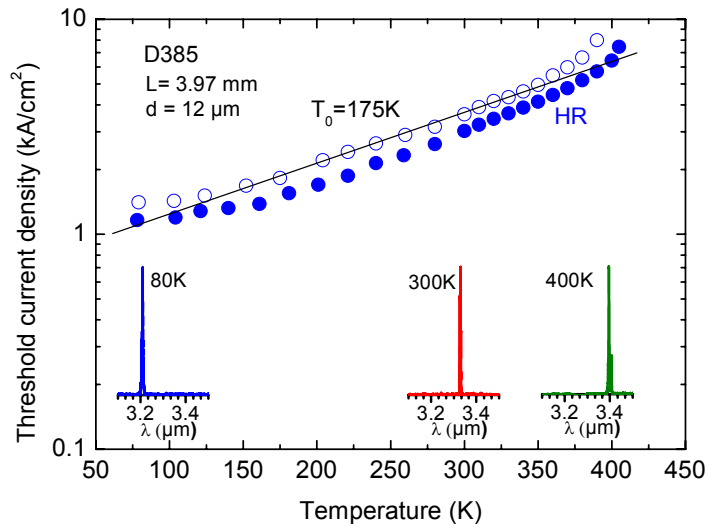


Fig. 6. Temperature dependence of the threshold current density of D385 lasers with (solid circles) and without HR coating (open circles) on back facets. Insets show emission spectra at different temperatures.

The temperature dependence of the threshold current density is presented in Fig.6 for HR coated and as cleaved devices. By using classical balance of gain and loss at threshold and assuming the HR coating reflectivity of 100%, we estimated the waveguide loss to be about  $5 \text{ cm}^{-1}$  from the data presented in Fig.6. The two curves in Fig.6 are nearly parallel, which means that the waveguide loss does not change with temperature.

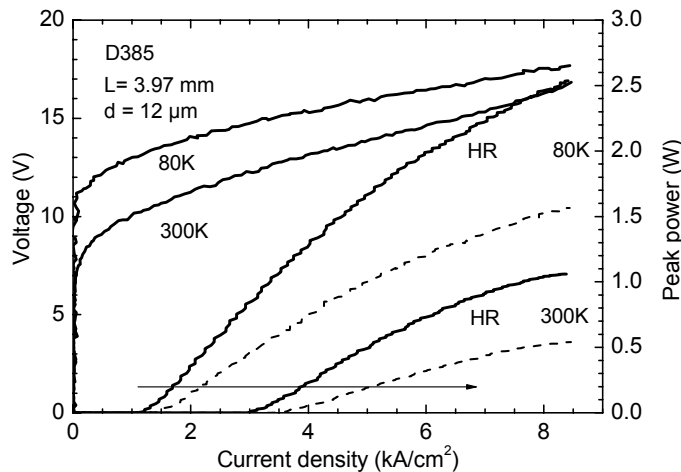


Fig. 7. Voltage-current and light-current characteristics of D385 lasers measured at 80 K and at RT. Dashed lines display characteristics of a device with uncoated facets.

The exponential increase of threshold current can be fitted with a characteristic temperature  $T_0 = 175 \text{ K}$ . The lasers operated in pulsed mode up to more than 400 K. At this temperature the emission wavelength shifted to  $4.4 \text{ μm}$  (insets in Fig.6). Voltage-current and light-current characteristics of D385 lasers are shown in Fig.7. At room temperature the maximum peak power of about 1 W and a slope efficiency of 500 mW/A have been obtained for the lasers with HR coated facets. We still get 110 mW of peak power and a slope efficiency of 100 mW/A at 380 K. The threshold current density is low, close to  $1 \text{ kA/cm}^2$  at cryogenic temperature and less than  $3 \text{ kA/cm}^2$  at room temperature. These performances are remarkable for such short wavelength QCLs. This validates the new design of the active regions and demonstrates that thermal backfilling was reduced and good injection efficiency was preserved at high temperature. Taking into account serial resistance of  $0.3 \text{ Ω}$ , the applied voltage at threshold is 12.0 V. It corresponds to a potential

drop of 520 meV per period, i.e. 150 meV more than the emitted photon energy. Such a large value is necessary for efficient high temperature operation.

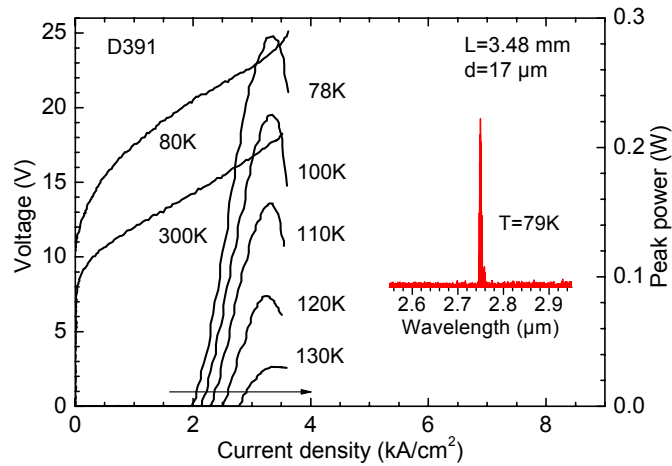


Fig. 8. Voltage-current and light-current characteristics and an emission spectrum of a D391 laser.

Figs.8 and 9 show voltage-current and light-current characteristics of QCLs fabricated from the wafers D391 and D392. The lasers D391 emitted at 2.75 µm at liquid nitrogen temperature (inset in Fig.8) with a threshold current density of 2 kA/cm<sup>2</sup>. The peak output power reached 0.3 W/facet at 78 K, the slope of the light-current

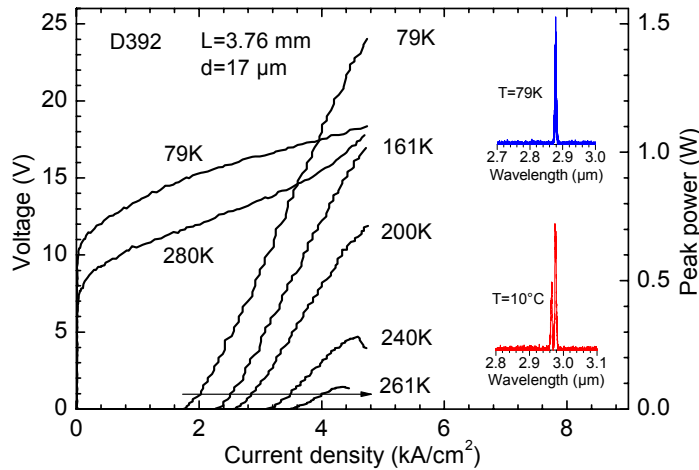


Fig. 9. Voltage-current and light-current characteristics of a D392 laser. Insets show emission spectra at different temperatures

characteristics being 0.7 W/A per facet. The maximum operation temperature for these devices was about 140 K. The lasers D392 exhibited a similar threshold current density at 80 K but operated up to 285 K in short pulse regime (40 ns). Their emission wavelength shifted from 2.88 µm at 80 K to 2.97 µm near room temperature (insets in Fig.9). The slope of the optical power versus current characteristics of 0.8 W/A at 79 K was close to that of the D391 lasers but the peak optical power exceeded 1.5 W/facet due to the larger current dynamic range.

Fig.10 displays the temperature dependence of the threshold current density of lasers with uncoated facets fabricated from all studied wafers. The most evident difference between these devices is the maximum operation temperature  $T_{max}$  which falls with reducing emission wavelength. The maximum available current density corresponding to the beginning

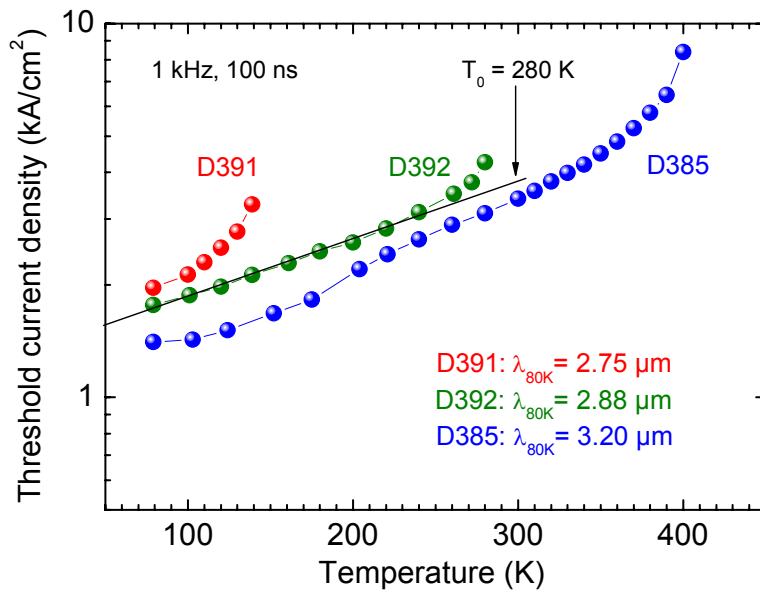


Fig. 10. Temperature dependence of threshold current density of QCLs emitting at different wavelengths.

of the rollover of light-current characteristics decreases from 9 to 5 and to 3 kA/cm<sup>2</sup> at 80 K in the lasers D385, D392 and D391, respectively. The laser D391 exhibits also stronger temperature dependence compared with other devices while low temperature thresholds are comparable for all of them. Different reasons concerning material properties, as well as the laser design can be responsible for the observed evolution of laser performances with emission wavelength.

## 5. DISCUSSION

Realization of short wavelength InAs/AlSb QCLs can be compromised by the small band gap of InAs and its type-II alignment with AlSb. The energy of interband transitions in the active region is quite close to the photon energy in InAs/AlSb QCLs emitting below 4 μm and the probability to absorb intersubband radiation is higher in short wavelength devices. The interband absorption should be stronger at high temperatures because its energy decreases faster with temperature than the intersubband photon energy. This mechanism can, in principle, be the origin of the poor temperature behavior of the D391 lasers. To reveal interband transitions in this structure its photoluminescence (PL) was studied. The samples with a typical size of 500x500 μm<sup>2</sup> were prepared from the unprocessed wafers, the upper cladding layer being removed by selective wet etching. The samples were soldered with In onto copper holders. A point contact to the upper spacer on the top of the samples allowed PL measurements under bias. A red diode laser was used for excitation at optical power density of about 10 W/cm<sup>2</sup>. PL spectra were recorded using the FTIR in the step scan regime and a cooled InSb detector. The dc bias applied to the samples in some measurements corresponded to the polarity of QCL operation, the current through the structure being negligible at the used voltage values. The PL spectra measured at RT are shown in Fig.11, as well as a spontaneous emission spectrum of a D391 laser (EL). The PL band near 0.82 eV is associated with the InAs/AlSb superlattice spacer, two other peaks (A and B) correspond to recombination of electrons from several bottom levels in the active zone of the structure. PL spectra of the D392 structure were similar but the distance between EL and A, B peaks was by 5-7 meV larger, in good agreement with calculated positions of electron levels. We attribute the PL band at 0.53 eV (A) to transitions involving acceptorlike states located at 80 meV above the valence band maximum of AlSb<sup>16</sup>. The peak at 0.67 eV (B) is supposed to be due to recombination with holes confined under injection barrier (right panel in Fig.11). Dashed vertical lines in the left panel of Fig.11 indicate expected low energy onsets of these PL bands calculated assuming a valence band offset between InAs and AlSb of 100 meV at 80 K<sup>16</sup>. Without bias photogenerated holes occupy the lowest energy state, that is, the acceptorlike levels in AlSb. When electric field is applied the holes can be detrapped from these states and populate the deepest hole well situated under injection barrier, which makes the B transition visible. No significant shift of these bands has been detected with bias up to a half of the turn-on voltage of the lasers. The relative intensity of the A transition decreased with bias, which is

consistent with the explanation given above. Whatever the origin of the observed interband transitions, they can not

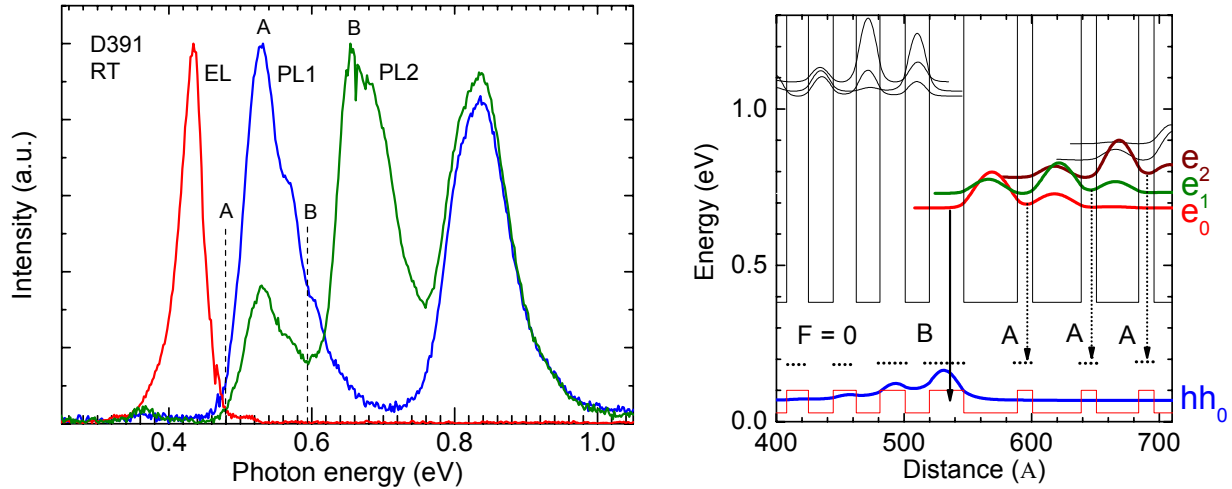


Fig. 11. Spontaneous emission spectrum (EL) and photoluminescence (PL) spectra of the D391 structure at room temperature and a scheme of interband transitions in the D391 structure without bias at room temperature. The PL spectra were measured without applied bias (PL1) and at a bias of 3 V with polarity corresponding to QCL operation (PL2). Dashed lines in the left panel display expected low energy onsets of the PL bands A and B.

perturb operation of the discussed devices as their energy is considerably higher than the intersubband photon energy even at RT.

The most discussed issue related to realization of short wavelength QCLs is the influence of the lateral valley in the conduction band of the well material on operation of the device<sup>4-6</sup>. If electron levels associated with the lateral valley, X- in InP-based material systems, or L-valley in InAs, are close to the excited state  $e_3$  of the laser transition they can upset functioning of the device. It should be noted, that the design employed in our last structures (Fig.5) results in not only reduced backfilling, but also in lower position of the  $e_3$  level. In the lasers D391 emitting at 2.75  $\mu\text{m}$  the  $e_3$  level is lower than in the structure D333 emitting at 2.95  $\mu\text{m}$  reported earlier<sup>6</sup>, which makes them less sensitive to the L-valley effect. According to different sources the  $\Gamma$ -L distance in InAs varies from 0.73 eV<sup>17</sup> to 1.13 eV<sup>18</sup>. The L-valley related states occur to be lower than upper levels of the laser transition in the structures D391 and D392, when calculated using the pessimistic data for the  $\Gamma$ -L separation. Comparison of the data presented in Fig.10 shows nevertheless no effect related to the L-valley at 80 K since the threshold current density does not depend significantly on emission wavelength. As the L-states move up slightly faster with electric field than levels participating in the lasing transition, it is also unlikely that the L-valley is responsible for the current limitation in the discussed devices at 80 K. On the other hand, the transfer of electrons into the indirect minimum becomes more probable with increasing temperature, which can explain the faster growth of the threshold in the D391 lasers.

Although the design of the discussed lasers is similar, the evolution of QCL properties with emission wavelength can be due to its details. We have found that coupling of the last injector state  $e_i$  with the preceding level  $e_{i-1}$  (see Fig.5) varies considerably in the different structures. The phonon limited electron lifetime in the level  $e_{i-1}$  at laser threshold conditions was calculated to be about 0.9, 2 and 3 ps in the structures D385, D392, and D391, respectively. Other injector levels are characterized by lifetimes shorter than 0.5 ps in all the samples. The maximum current through a QCL is limited primarily by the doping level which was the same in these structures. As in the samples D391 and D392 the lifetime in the level  $e_{i-1}$  is very long, it accumulates electrons thus limiting the current despite the same number of electrons. The evolution of the maximum available current in the discussed lasers is consistent with this analysis. We suppose the operation temperature of the D391 and D392 lasers to be limited by the small available current while the poor temperature behavior of the D391 lasers can be explained by the proximity of the current limitation region. Performances of these devices can be improved by optimization of the injector region.

## 5. CONCLUSION

We realized high performance QCLs emitting near 3.3  $\mu\text{m}$  with pulsed output powers of 1 W at room temperature and operating up to 400 K. We demonstrated QCLs emitting at wavelengths as short as 2.75  $\mu\text{m}$ , a new short wavelength frontier of QCL operation. Our results show that interband transitions in the QCL active zone across the small band gap of InAs do not affect performances of these devices. Electron scattering into L-valley related states in InAs wells does not influence operation of the short wavelength InAs/AlSb QCLs, at least at low temperatures.

A plasmon enhanced waveguide was shown to be suitable for InAs-based QCLs emitting near 3  $\mu\text{m}$  or even below this mark. The waveguide loss in such lasers, due essentially to free carrier absorption in heavily doped cladding layers, was found to be about 5  $\text{cm}^{-1}$ .

## REFERENCES

- <sup>1</sup> A. Evans, S. R. Darvish, S. Slivken, J. Nguyen, Y. Bai, and M. Razeghi, *Appl. Phys. Lett.* **91**, 071101 (2007).
- <sup>2</sup> J. S. Yu, A. Evans, S. Slivken, S. R. Darvish, and M. Razeghi, *Appl. Phys. Lett.* **88**, 251118 (2006).
- <sup>3</sup> J. Faist, F. Capasso, D. L. Sivco, C. Sirtori, A. L. Hutchinson, and A. Y. Cho, *Science*, **264**, 553, (1994)
- <sup>4</sup> M. P. Semtsiv, M. Wienold, S. Dressler, and W.T. Masselink, *Appl. Phys. Lett.* **90**, 051111 (2007).
- <sup>5</sup> D. G. Revin, J. W. Cockburn, M. J. Steer, R.J.Airey, M.Hopkinson, A.B.Krysa, L. R. Wilson, S.Menzel, *Appl. Phys. Lett.* **90**, 021108 (2007).
- <sup>6</sup> J. Devenson, R. Teissier, O. Cathabard, and A.N. Baranov, *Appl. Phys. Lett.* **90**, 111118 (2007).
- <sup>7</sup> C. Sirtori, P. Kruck, S. Barbieri, H. Page, and J. Nagle; M. Beck, and J. Faist, *Appl. Phys. Lett.* **75**, 3911 (1999).
- <sup>8</sup> K. Ohtani and H. Ohno, *Jpn. J. Appl. Phys.* **41**, L1279 (2002).
- <sup>9</sup> M. Grau, C. Lin, O. Dier, C. Lauer, and M.-C. Amann, *Appl. Phys. Lett.* **87**, 241104 (2005).
- <sup>10</sup> R. Teissier, D. A. Yarekha, A. Vicet, D. Barate, P. Grech, P. Christol, C. Alibert et A. N. Baranov; C. Becker, X. Marcadet, M. Garcia et C. Sirtori, paper A-3.26, JNMO (St Aygulf, France, 29<sup>th</sup> September – 2<sup>nd</sup> October, 2002).
- <sup>11</sup> P. Y. Yu, M. Cardona, *Fundamentals of Semiconductors*, Springer, Berlin, 1996.
- <sup>12</sup> R. Teisser, D. Barate, A. Vicet, C. Alibert, A. N. Baranov, X. Marcadet, C. Renard, M. Garcia, C. Sirtori, D. Revin, J. Cockburn, *Appl. Phys. Lett.* **85**, 167 (2004).
- <sup>13</sup> K. C. Wong, C. Yang, M. Thomas and H-R Blank, *J. Appl. Phys.* **82**, 4904 (1997).
- <sup>14</sup> C. Renard, X. Marcadet, J. Massies, I. Prévot, R. Bisaro and P. Galtier, *J. Cryst. Growth* **259**, 69 (2003).
- <sup>15</sup> J. Devenson, R. Teissier, O. Cathabard, and A. N. Baranov, *Appl. Phys. Lett.* **89**, 191115 (2006).
- <sup>16</sup> F. Fuchs, J. Schmitz, H. Obloh, J. D. Ralston, and P. Koidl, *Appl. Phys. Lett.* **64** (13), 1665 (1994).
- <sup>17</sup> I. Vurgaftman, J. R. Meyer, and L. R. Ram-Mohan, *J. Appl. Phys.* **89**, 5815, (2001).
- <sup>18</sup> G. W. Charache, D. M. DePoy, J. E. Reynolds, P. F. Baldasaro, K. E. Miyano, T. Holden, F. H. Pollak, P. R. Sharps, M. L. Timmons, C. B. Geller, W. Mannstadt, R. Asahi, A. J. Freeman, and W. Wolf, *J. Appl. Phys.* **86**, 452 (1999).